The Astronomical Journal, 124:1258–1265, 2002 September

STAR FORMATION HISTORY SINCE $z = 1.5$ AS INFERRED FROM REST-FRAME ULTRAVIOLET LUMINOSITY DENSITY EVOLUTION

Gillian Wilson,[1,2] Lennox L. Cowie,[3] Amy J. Barger,[3,4,5] and D. J. Burke[3,6]

Received 2001 August 27; accepted 2002 May 13

ABSTRACT

We investigate the evolution of the universal rest-frame ultraviolet luminosity density from $z = 1.5$ to the present. We analyze an extensive sample of multicolor data (U'_{AB}, B_{AB}, $V_{AB} = 24.5$) plus spectroscopic redshifts from the Hawaii Survey Fields and the Hubble Deep Field. Our multicolor data allow us to select our sample in the rest-frame ultraviolet (2500 Å) over the entire redshift range to $z = 1.5$. We conclude that the evolution in the luminosity density is a function of the form $(1 + z)^{1.7 \pm 1.0}$ for a flat lambda ($\Omega_{m0} = 0.3$, $\Omega_{\lambda 0} = 0.7$) cosmology and $(1 + z)^{2.4 \pm 1.0}$ for an Einstein–de Sitter cosmology.

Key words: cosmology: observations — galaxies: distances and redshifts — galaxies: evolution — galaxies: formation — galaxies: luminosity function, mass function

1. INTRODUCTION

A major goal of observational cosmology is to understand the star formation history of the universe from the earliest epoch of structure formation to the present. Much recent attention has focused on determining the contribution to the global history from the most distant sources; however, the star formation history, even at modest redshifts ($z < 1$), is not well determined and has recently undergone a revision.

Early work by Madau et al. (1996; later updated by Madau, Pozzetti, & Dickinson 1998) suggested that the global star formation as seen in the optical and ultraviolet (UV) had a strong peak around $z = 1$ and then fell very steeply at lower redshifts. The $z < 1$ data used in the analysis were taken from a paper by Lilly et al. (1996), who used rest-frame near-UV luminosities derived from the *I*-selected Canada-France Redshift Survey (CFRS; Lilly et al. 1995) to determine the comoving UV luminosity density from $z = 1$ to the present. These authors found the evolution to be a steep function of the form $(1 + z)^4$. However, when Treyer et al. (1998) presented the first UV-selected constraints on the local integrated luminosity density, they found that their result was well above the optically derived estimates. Sullivan et al. (2000) subsequently tripled the Treyer et al. UV-selected sample and confirmed the higher local volume-averaged star formation rate.

Cowie, Songaila, & Barger (1999, hereafter CSB99) decided to reinvestigate the rest-frame UV luminosity density evolution to $z = 1$ using a large, extremely deep, and highly complete spectroscopic galaxy redshift survey. Their data enabled them to select objects based on the rest-frame UV magnitudes at all redshifts. The evolution found by these authors was a much shallower function of the form $(1 + z)^{1.5}$. CSB99 suggested that the differences between their results and those of Lilly et al. could be accounted for by the *I*-band selection of the Lilly et al. sample, which required large extrapolations to obtain UV colors, and by the CFRS data not being deep enough to probe the flat segments of the luminosity function (LF), which meant that at redshifts near $z = 1$ reliable extrapolations to total luminosity density could not be made.

In this paper, we expand on the work of CSB99 to more thoroughly investigate the rest-frame UV luminosity density evolution from $z = 1.5$ to the present. Our new galaxy sample is nearly twice as large as that used by CSB99, and we explore various methods for constructing the UV LFs. The outline of the paper is as follows. In § 2, we present our data sample and strategy and investigate the U' number counts and redshift distribution. We also explore the redshift-magnitude relationship for the U', B, and V passbands. In § 3, we describe how we construct rest-frame UV LFs as a function of redshift from the U', B, and V data. In § 4, we use these LFs to infer the evolution of the global UV luminosity density with redshift. In § 5, we summarize our conclusions. Initially, we assume a flat lambda ($\Omega_{m0} = 0.3$, $\Omega_{\lambda 0} = 0.7$) cosmology with $H_0 = 100\,h$ km s^{-1} Mpc^{-1}. Subsequently, we investigate the effect of an Einstein–de Sitter ($\Omega_{m0} = 1.0$, $\Omega_{\lambda 0} = 0.0$) cosmology on our results.

2. OBSERVATIONS

We analyzed a three passband subset (U' [3400 ± 150 Å], B, V) of an ongoing eight passband (U', B, V, R, I, Z, J, and HK') Hawaii imaging survey of four $6' \times 2'.5$ areas crossing the Hawaii Survey Fields SSA 13, SSA 17, and SSA 22 (Lilly, Cowie, & Gardner 1991) and the Hubble Deep Field (HDF; Williams et al. 1996). The B and V images were obtained using the Low-Resolution Imaging Spectrograph (LRIS; Oke et al. 1995) on the Keck 10 m telescopes and the UH8K CCD Mosaic Camera (Luppino 1998) on the Canada-France-Hawaii 3.6 m telescope. The U' data were taken with the ORBIT CCD on the University of Hawaii 2.2 m telescope. All magnitudes were measured in $3''$ diameter apertures and corrected to total magnitudes following the procedures described in Cowie et al. (1994).

[1] Department of Physics, Brown University, 182 Hope Street, Providence, RI 02912.
[2] SIRTF Science Center, M/S 220-6, California Institute of Technology, 1200 East California Boulevard, Pasadena, CA 91125.
[3] Institute for Astronomy, University of Hawaii, 2680 Woodlawn Drive, Honolulu, HI 96822.
[4] Department of Astronomy, University of Wisconsin–Madison, 475 North Charter Street, Madison, WI 53706.
[5] Hubble Fellow and Chandra Fellow at Large.
[6] Harvard-Smithsonian Center for Astrophysics, 60 Garden Street, Cambridge, MA 02138.

The Johnson V and B magnitudes were photometrically calibrated using Landolt standards, while the narrowband filter at 3400 Å was calibrated using spectrophotometric standards in the AB system. The offsets between AB magnitudes and the Vega-based magnitudes are 0.0 and −0.11 for V and B, respectively, where the AB magnitude is defined as $-48.60 - 2.5 \log f_\nu$. Here f_ν is the flux of the source in units of ergs $\mathrm{cm}^{-2}\,\mathrm{s}^{-1}\,\mathrm{Hz}^{-1}$.

Spectra were obtained with the LRIS on the Keck 10 m telescope in multislit mode (Oke et al. 1995), supplemented in the case of the HDF with redshifts from the literature compiled in the catalog of Cohen et al. (2000). We used 1.″4 wide slits throughout. Initially, we used the 300 lines mm^{-1} grating blazed at 5000 Å, which gives a wavelength resolution of ∼16 Å and a wavelength coverage of ∼5000 Å. The wavelength range for each object depends on the exact location of the slit in the mask but is generally between ∼5000 and 10000 Å. After the blue side of LRIS was implemented, we used the 400 lines mm^{-1} grating on the red side and the 600 lines mm^{-1} grism on the blue side, split by the 560 dichroic. This gives a slightly higher resolution spectrum (∼12 Å) and nearly complete wavelength coverage from ∼3500 to 10000 Å. The observations were taken with exposure times of 1–1.5 hr per slit mask. Each exposure was broken into three subsets with the objects stepped along the slit by 2″ in each direction, and the sky backgrounds were removed using the median of the images to avoid the difficult and time-consuming problems of flat-fielding LRIS data. Fainter objects were observed a number of times with the maximum exposure time for an individual source around 6 hr. Details of the spectroscopic reduction procedures can be found in Cowie et al. (1996).

The sources analyzed in this paper contain and extend the CSB99 catalogs. The total number of galaxies with spectroscopic redshifts in the present U', B, and V samples are 403, 414, and 518, all to a survey limit magnitude (AB) of 24.5. These numbers can be compared to those in CSB99 (218, 350, and 259, respectively). Thus, our current data set contains approximately double the number of objects in the CSB99 U' and V samples.

The great advantage of multiband data is that one can, for all redshifts, select galaxies based on their rest-frame UV magnitudes, thereby avoiding the uncertainties associated with selecting galaxies at longer (redder) wavelengths and then extrapolating to obtain their UV magnitudes. In addition, the depth of the current data set allows us to construct LFs to sufficiently faint absolute magnitudes to constrain the faint-end slope. Moreover, by selecting galaxies based on their rest-frame UV magnitudes, we expect the relative shape of the inferred UV LFs to be minimally sensitive to the effect of interstellar dust; i.e., we expect the relative forms of our derived LFs (and hence the relative values of our luminosity densities) to be subject only to evolution in the amount or properties of galactic dust with redshift and not to its effect in absolute terms. (Note that any potentially much larger correction for dust extinction *within* the distant star-forming galaxy should not be confused with the usual tiny correction made for extinction by interstellar dust using Burstein & Heiles 1984.)

As discussed in CSB99, one is free to choose the rest-frame wavelength at which to compute LFs and the UV light density. For our data set, 2500 Å provides a sensible compromise between our wide range of redshifts and large number of galaxies in each passband.

In each sample, there are galaxies that were not spectroscopically observed or for which no redshift could be reliably determined from the spectrum obtained. We construct LFs either by omitting them (i.e., we assume they are unidentified because they are unusual in some way, e.g., at very high redshift) or by assuming they are distributed in redshift in exactly the same manner as the identified galaxies (i.e., we assume they are identical to the measured galaxies but have been missed for some trivial reason, e.g., impractical slit-mask geometry such as close proximity to neighboring galaxies). It is likely that the true LF lies between these two possibilities. In subsequent sections, we refer to the former case as minimal and the latter case as incompleteness-corrected. The U', B, and V samples are 88%, 90%, and 83% complete, respectively, so the correction is not a huge factor in any case.

2.1. *The U' Sample*

Figure 1 shows number counts versus apparent magnitude for our U' sample. The symbols indicate the number counts in each of the four fields. We assume a 1 σ Poisson uncertainty for each field. The solid line shows the best fit to the counts for galaxies with U' magnitudes between 22.0 and 24.0 (slope of 0.61 ± 0.06 and intercept at -10.34 ± 1.49). The uncertainties were calculated from the field-to-field variations.

A number of groups (e.g., Williams et al. 1996; Pozzetti et al. 1998; Gardner, Brown, & Ferguson 2000) have measured deep galaxy counts at 3000 Å from the *HST* Hubble Deep Field imaging survey, but their counts are somewhat deeper than those presented here, so it is difficult to make a direct comparison. The sample most similar to ours was that obtained at the Palomar 5 m by Hogg et al. (1997). We overplot their data (*filled diamonds*) on Figure 1 for comparison, after converting their magnitudes to U'_{AB} by adding 0.79 mag. The agreement is generally good.

In Figure 2, we show the total number of objects in our U' sample versus redshift for two apparent magnitude bins. The top panel shows the number of galaxies versus redshift for all galaxies with U' magnitudes between 22.5 and 23.5,

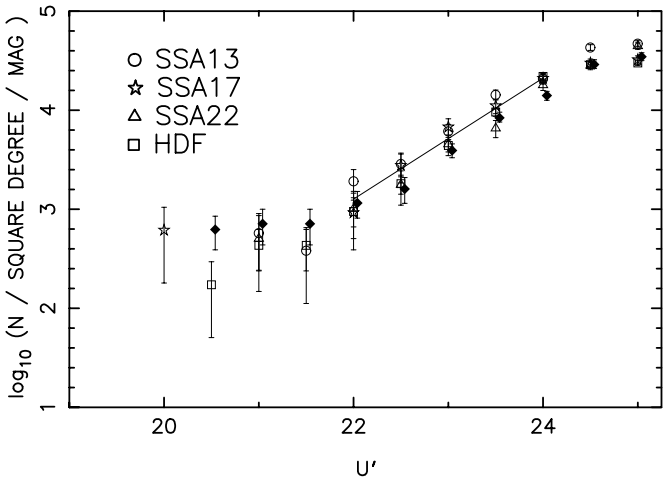

FIG. 1.—Number counts vs. apparent magnitude for the U' sample. The four fields are as indicated by the key. The solid line shows the best fit to the U' counts between 22.0 and 24.0 (slope of 0.61 and intercept at −10.34). The filled diamonds are the counts from Hogg et al. (1997).

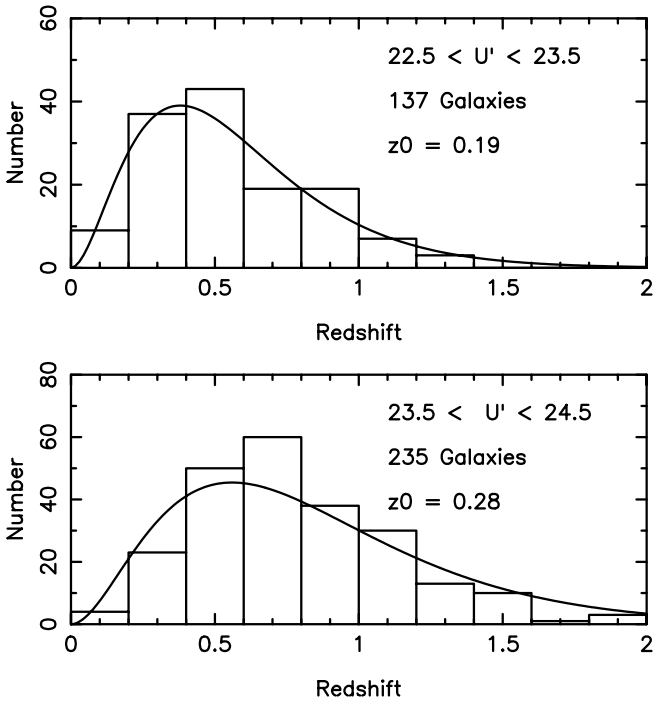

FIG. 2.—Redshift distributions for the U' sample. The top panel shows $N(z)$ for a 1 mag wide band ($22.5 < U' \leq 23.5$) in apparent magnitude. At this depth, the data are 97% complete. The solid line shows the best fit to the model (eq. [1]) with a redshift scale parameter of 0.19. The bottom panel shows $N(z)$ for $23.5 < U' \leq 24.5$. At this depth, the data are 87% complete and best fit with a redshift scale parameter of 0.28.

and the bottom panel is for galaxies with U' magnitudes between 23.5 and 24.5.

Wilson et al. (2001) found that a good model for the redshift distribution (at least at I and V) is provided by

$$p(z) = 0.5z^2 \exp(-z/z_0)/z_0^3 , \quad (1)$$

where $p(z)dz$ is the probability of finding a galaxy in the redshift interval $z + dz$ (the mean redshift is $\overline{z} = 3z_0$, and the median redshift is $z_{\rm median} = 2.67z_0$). A nice property of equation (1) is that there is only one free parameter, the redshift scale parameter z_0. The solid lines overlaid on Figure 2 show the best fits to the model ($z_0 = 0.19$ and 0.28), normalized to the total number of galaxies in each sample.

2.2. *Magnitude-Redshift Dependence*

In this section, we investigate the dependence of median redshift on apparent magnitude and wavelength. In Figure 3, we show redshift versus magnitude for the U' sample. The symbols denote the field in which the galaxy was observed. Note that the SSA 13, SSA 22, and HDF fields are ~90% complete to an AB limiting magnitude of 24.5, and the SSA 17 field is similarly complete to 23.5.

Table 1 quantifies Figure 3, giving the median redshift with ± 1 σ Poisson uncertainties (Gehrels 1986) and the number of objects in each half-magnitude interval as a function of apparent magnitude. We note that the median redshift obtained from the parameterized fit to the data (eq. [1]) for the $22.5 < U' \leq 23.5$ interval is 0.51, and for the $23.5 < U' \leq 24.5$ interval, 0.75. The values are in good agreement with those calculated directly in Table 1.

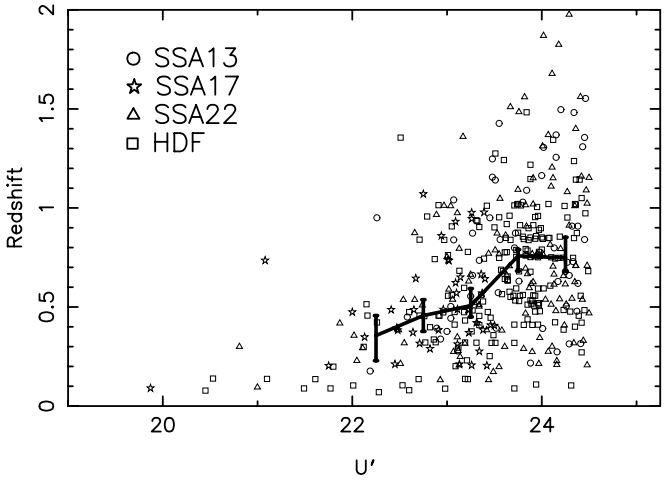

FIG. 3.—Galaxy redshift vs. apparent magnitude for the U' sample. The key is as in Fig. 1. The solid line shows the median redshift and the 1 σ Poisson uncertainties (Table 1).

In Table 1, we also calculate the median redshift for the B and V samples. Median redshift as a function of apparent magnitude can potentially be used to constrain galaxy evolution models, e.g., if we compare with the B-band predictions from the merger model proposed by Carlberg (1992, his Table 2), we find that his median redshift values of 0.44 for $B = 23$ and 0.55 for $B = 24$ are lower than our values, suggesting that more pure luminosity evolution might have occurred than was proposed in his model.

3. THE REST-FRAME ULTRAVIOLET LUMINOSITY FUNCTION

For any given galaxy, i, at redshift, z, the equation relating the absolute and apparent magnitudes is given by

$$M_i^{2500} = m_i - 5\log d_L(z) - 25 + 2.5\log(1+z) + dK(z) , \quad (2)$$

where m is the observed magnitude at the redshifted wavelength and $d_L(z)$ is the luminosity distance in h^{-1} Mpc. The quantity $dK(z)$ is given by

$$dK(z) = 2.5\log\frac{f_\nu[(2500\ \text{Å})(1+z)]}{f_\nu[(2500\ \text{Å})(1+z_c)]} , \quad (3)$$

where f_ν is the spectral energy distribution of the galaxy and z_c is the redshift corresponding to the center of the band. The differential K-correction, $dK(z)$, allows for each sample containing a range of redshifts and hence a range of rest-frame wavelengths around 2500 Å. It is generally small and is obtained by interpolation from the neighboring passbands.

3.1. *LFs from the V_{max} Method*

We used two methods to construct LFs: the traditional $V_{\rm max}$ method described by Schmidt (1968), Felten (1976), and Ellis et al. (1996) and a new method recently suggested by Page & Carrera (2000). In the $V_{\rm max}$ method, the number density of galaxies in the redshift range $[z_1, z_2]$ with absolute

TABLE 1
MEDIAN REDSHIFTS AND GALAXY NUMBERS AS A FUNCTION OF APPARENT MAGNITUDE AND WAVELENGTH

Magnitude	$z_{\rm med}(U')$	$N(U')$	$z_{\rm med}(B)$	$N(B)$	$z_{\rm med}(V)$	$N(V)$
22.25	$0.356^{+0.457}_{-0.229}$	17	$0.380^{+0.452}_{-0.317}$	44	$0.411^{+0.471}_{-0.348}$	45
22.75	$0.457^{+0.537}_{-0.377}$	43	$0.475^{+0.560}_{-0.432}$	55	$0.475^{+0.524}_{-0.455}$	65
23.25	$0.507^{+0.593}_{-0.450}$	94	$0.663^{+0.777}_{-0.564}$	86	$0.626^{+0.742}_{-0.531}$	113
23.75	$0.758^{+0.790}_{-0.682}$	127	$0.715^{+0.788}_{-0.617}$	112	$0.680^{+0.753}_{-0.615}$	141
24.25	$0.748^{+0.852}_{-0.680}$	108	$0.753^{+1.010}_{-0.562}$	77	$0.850^{+0.980}_{-0.709}$	104

NOTE.—The uncertainties are 1 σ Poissonian limits.

magnitude M is given by

$$\phi(M)dM = \sum \frac{1}{V_{\rm max}(M)} , \quad (4)$$

where the sum is over the galaxies in the magnitude interval $M \pm dM/2$. $V_{\rm max}(M)$ is the maximum total comoving volume within which each galaxy (as defined by its apparent magnitude and redshift) would remain detectable within survey limits. The uncertainty for each magnitude interval is conventionally calculated from

$$\sigma = \left\{ \sum \frac{1}{[V_{\rm max}(M)]^2} \right\}^{1/2} \quad (5)$$

(Marshall 1985; Boyle, Shanks, & Peterson 1988). This expression weights each observation by its contribution to the sum. However, it assumes Gaussian statistics, which is not ideal for bins at the bright or faint end of the LF where only a small number of objects contribute to the sum.

Figure 4 shows the 2500 Å rest-frame LF for our three redshift bins: $z = 0.2$–0.5, constructed from the U' sample (*top panel*); $z = 0.6$–1.0, constructed from the B sample (*center panel*); and $z = 1.0$–1.5, constructed from the V sample (*bottom panel*). At redshifts $z = 0.35 \pm 0.15$, 0.80 ± 0.20, and 1.25 ± 0.25, the U' (3400 Å), B (4500 Å), and V (5500 Å) samples correspond to rest-wavelengths of 2519^{+314}_{-253}, 2500^{+312}_{-250}, and 2444^{+306}_{-244} Å. The open circles denote the minimal function, and the filled circles denote the incompleteness-corrected function. The number of galaxies used in the construction of each LF was 121 (U'), 119 (B), and 59 (V).

3.2. *LFs from the Page-Carrera Method*

The Page & Carrera (2000) method is very similar to the $V_{\rm max}(M)$ method in that it results in a binned differential LF, but the advantage is that it more accurately determines the LF at the faint end. The maximum redshift at which any galaxy may be found is a constantly varying function determined by the flux limit of the survey. The $V_{\rm max}(M)$ method assumes that the redshift is a constant for any given absolute magnitude bin. However, by dividing each magnitude bin into a series of steps, calculating $V_{\rm max}(M)$ for each interval, and then integrating over the magnitude bin, one can obtain a more precise estimate of the maximum volume to which each object could be observed in the survey. Estimates of $\phi(M)$ obtained by either of the two methods should agree at the bright end of the LF where objects are much brighter than the flux limit. The two estimates should also agree in the case of very fine magnitude intervals, such that the widths of the magnitude bins tend to zero.

We denote the LFs obtained using the $V_{\rm PC}$ method by diamonds in Figure 4. The open triangles show the minimal function and the filled triangles show the incompleteness-corrected function. The diamonds have been offset from the circles of the $V_{\rm max}$ method by 0.15 mag for clarity. The $\pm 1\ \sigma$ Poisson uncertainties (Gehrels 1986) in the LFs are appropriate for small numbers of objects per magnitude interval. The LFs obtained from the two methods are very similar.

Both $V_{\rm max}(M)$ and $V_{\rm PC}(M)$ give unbiased estimates of $\phi(M)$ only if galaxy clustering can be neglected. It is easy to

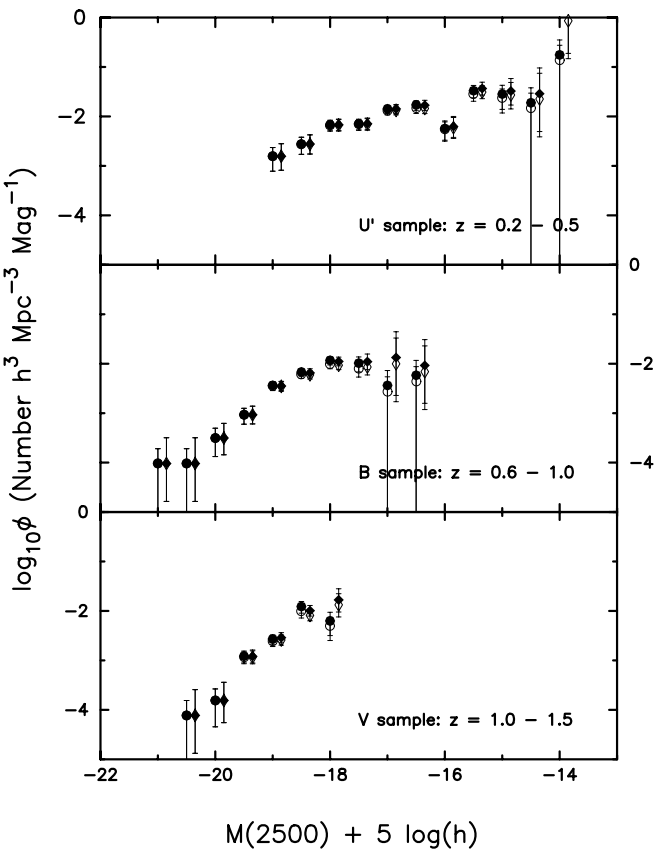

FIG. 4.—The 2500 Å rest-frame LF for three redshift bins: $z = 0.2$–0.5 (2250–2850 Å) from the U' sample (*top*), $z = 0.6$–1.0 (2250–2800 Å) from the B sample (*center*), and $z = 1.0$–1.5 (2200–2750 Å) from the V sample (*bottom*). An $\Omega_{m0} = 0.3$, $\Omega_{\lambda 0} = 0.7$ cosmology is assumed. The open circles denote the minimal function, and the filled circles denote the incompleteness-corrected function obtained using the $V_{\rm max}$ method. The diamonds (offset by 0.15 mag for clarity) show the minimal (*open*) and incompleteness-corrected (*filled*) functions obtained using the $V_{\rm PC}$ method. See text for details and an explanation of the uncertainties. For this data set, the LFs obtained from the two methods are very similar.

imagine how a nearby excess of clustering could bias the estimator: such an excess of intrinsically faint galaxies would cause the LF to be too steep at the faint end. Although the effects of clustering are mostly of concern in pencil-beam surveys, we tested two maximum likelihood alternatives, which should be less sensitive to clustering, on our U' sample. These were the Schechter fit estimator suggested by Sandage, Tammann, & Yahil (1979) and the stepwise estimator of Efstathiou, Ellis, & Peterson (1988). In all cases, the LFs were very similar to those obtained using $V_{\max}$, giving us confidence in the robustness of our results. We also note that the LFs in this paper were obtained using code written independently from that used in CSB99.

3.3. *Schechter Parameterization*

We then assumed that each LF could be parameterized by a Schechter function

$$\phi(M)dM = k\phi^* e^{k(\alpha+1)(M^*-M)} e^{-e^{k(M^*-M)}}\, dM\ , \qquad (6)$$

where $k = \frac{2}{5}\ln 10$ (Schechter 1976). We solved for the best-fit Schechter parameters assuming two fixed faint-end slopes that likely bound the range of faint-end slopes: $\alpha = -1.0$ and -1.5. Table 2 shows the best-fit absolute magnitude at the knee (M^*) and normalization (ϕ^*) for these values of fixed faint-end slope. In Figure 5, the open circles again show the minimal function; the filled circles show the incompleteness-corrected function assuming a flat lambda cosmology as in Figure 4. Overlaid on Figure 5 are the best-fitting Schechter functions assuming $\alpha = -1.0$ or -1.5. The solid portion of the line shows the magnitude range used in the fit.

3.4. *Effect of Cosmology*

We then investigated how one's choice of cosmology affects the LFs. We reconstructed LFs again using the $V_{\max}(M)$ method, but this time assuming an Einstein–de Sitter cosmology. For comparison, in Figure 5, the open triangles show the minimal function; the filled triangles show the incompleteness-corrected function assuming this cosmology. As in Figure 4, the triangles have been offset by 0.15 mag for clarity.

Table 3 shows the best-fit Schechter values of absolute magnitude at the knee (M^*) and normalization (ϕ^*) for the Einstein–de Sitter cosmology (again assuming fixed faint-end slopes of -1.0 and -1.5). From Figure 5 and from Tables 2 and 3, it is clear that the larger distances and volumes associated with a cosmological constant cause M^* and ϕ^* to decrease compared with the best-fit parameters in the Einstein–de Sitter case.

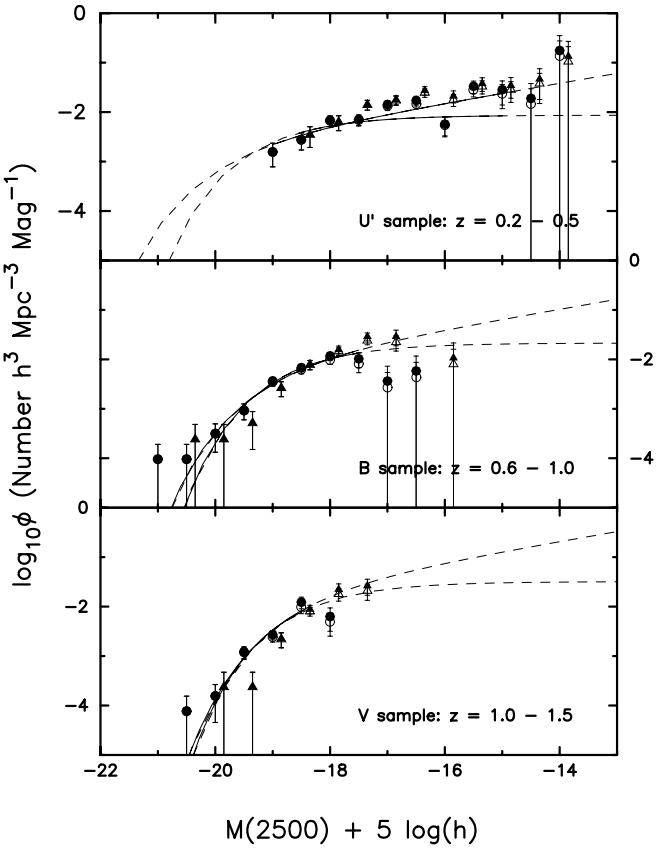

FIG. 5.—Circles as in Fig. 4 for a $\Omega_{m0} = 0.3$, $\Omega_{\lambda 0} = 0.7$ cosmology. Overlaid are the best-fitting Schechter functions assuming either $\alpha = -1.0$ or -1.5. The solid portion of the line shows the magnitude range used in the fit. Also shown and denoted by the triangles (offset by 0.15 mag for clarity) are the minimal (*open*) and incompleteness-corrected (*filled*) functions obtained for an Einstein–de Sitter cosmology. See text for details. See Tables 2 and 3 for best Schechter function fit parameters.

4. REST-FRAME UV LUMINOSITY DENSITY EVOLUTION

The LFs in § 3 can now be used to calculate the rest-frame ultraviolet luminosity densities, $\mathscr{L}$, with redshift. One

TABLE 2

SCHECHTER FUNCTION PARAMETER FITS FOR MINIMAL AND INCOMPLETENESS-CORRECTED POINTS FOR FLAT LAMBDA COSMOLOGY

		$\alpha = -1.0$			$\alpha = -1.5$			
SAMPLE	CORRECTED?	M^*	ϕ^*	χ^2/ν	M^*	ϕ^*	χ^2/ν	RANGE
U'.....	No	−18.17	0.0142	1.90	−19.86	0.0024	2.51	[−19.25, −14.75]
	Yes	−18.08	0.0161	1.25	−19.64	0.0031	1.58	[−19.25, −14.75]
B.....	No	−18.46	0.0178	0.55	−18.96	0.0089	0.86	[−21.25, −17.25]
	Yes	−18.34	0.0232	0.20	−18.81	0.0123	0.36	[−21.25, −17.25]
V.....	No	−18.30	0.0212	0.87	−18.53	0.0183	0.75	[−20.75, −18.25]
	Yes	−18.12	0.0348	0.69	−18.35	0.0306	0.58	[−20.75, −18.25]

NOTE.—The columns show the best-fit values of absolute magnitude at the knee (M^*), normalization (ϕ^*), and reduced χ^2 for fixed faint-end slope (α) of -1.0 and -1.5.

TABLE 3
SCHECHTER FUNCTION PARAMETER FITS FOR MINIMAL AND INCOMPLETENESS-CORRECTED POINTS FOR EINSTEIN–DE SITTER COSMOLOGY

		$\alpha = -1.0$			$\alpha = -1.5$			
SAMPLE	CORRECTED?	M^*	ϕ^*	χ^2/ν	M^*	ϕ^*	χ^2/ν	RANGE
U'.....	No	−17.64	0.0322	0.41	−19.02	0.0070	0.88	[−18.75, −14.75]
	Yes	−17.52	0.0378	0.22	−18.75	0.0094	0.41	[−18.75, −14.75]
B.....	No	−17.86	0.0512	0.26	−18.23	0.0318	0.25	[−20.75, −17.25]
	Yes	−17.75	0.0643	0.09	−18.13	0.0405	0.05	[−20.75, −17.25]
V.....	No	−17.63	0.0812	0.19	−17.85	0.0699	0.21	[−20.25, −17.75]
	Yes	−17.54	0.1100	0.04	−17.78	0.0932	0.04	[−20.25, −17.75]

NOTE.—The columns show the best-fit values of absolute magnitude at the knee (M^*), normalization (ϕ^*), and reduced χ^2 for fixed faint-end slope (α) of −1.0 and −1.5.

approach is to choose a magnitude limit and to sum the LF over the magnitude bins directly using

$$\mathscr{L}_{\rm direct} = 4.4 \times 10^{20} \sum \frac{10^{-0.4M}}{V_{\rm max}(M)}\ h \text{ ergs s}^{-1}\text{ Hz}^{-1}\text{ Mpc}^{-3}\ . \quad (7)$$

An alternative approach, which we adopt, is to choose a faint-end slope (we use either $\alpha = -1.0$ or -1.5) and to integrate the LF analytically using the best-fit Schechter parameters from Tables 2 and 3

$$\mathscr{L}_{\rm Schechter} = \int_0^\infty L\phi(L)dL = L^*\phi^*\Gamma(\alpha + 2)\ , \quad (8)$$

giving

$$\mathscr{L}_{\rm Schechter} = (4.4 \times 10^{20}) \times 10^{-0.4M^*}\phi^*\Gamma(\alpha + 2)\ h \quad (9)$$

in units of ergs s^{-1} Hz^{-1} Mpc^{-3}.

Although this method involves integrating over all luminosities, fainter galaxies have a rapidly decreasing contribution to the total luminosity density, and thus the two methods give similar results. We calculate the luminosity density for both the minimal and incompleteness-corrected cases assuming first a faint-end slope of $\alpha = -1.0$ and then $\alpha = -1.5$. The resulting luminosity densities for the flat lambda and Einstein–de Sitter cosmologies are shown in Table 4.

Luminosity density evolution with redshift is often parameterized as a power law, $\mathscr{L} \propto (1 + z)^\beta$. In Figure 6, we show log (luminosity density) versus log $(1 + z)$ using the values from Table 4. As in Figure 5, we use circles to denote the flat lambda cosmology and triangles to denote the Einstein–de Sitter cosmology. The open symbols denote the minimal case, and the filled symbols denote the incompleteness-corrected case.

We solved for the best-fit power-law exponent, β, in each case. We used the mean of the luminosity densities obtained assuming faint-end slopes of $\alpha = -1.0$ and -1.5 as our best estimate, with the extreme values as estimates of the uncertainty. Table 5 gives the best-fit exponent and uncertainty as a function of completeness-correction and cosmology. For the flat lambda cosmology, we found a best-fit exponent of 1.44 ± 0.63 in the minimal case and a best-fit exponent of 1.95 ± 0.65 in the incompleteness-corrected case. For the Einstein–de Sitter cosmology, we found a best-fit exponent of 2.22 ± 0.62 in the minimal case and a best-fit exponent of 2.54 ± 0.62 in the incompleteness-corrected case. Thus, depending on the choice of completeness correction, we conclude that luminosity density evolves as $(1 + z)^{1.7 \pm 1.0}$ in the $\Omega_{m0} = 0.3$, $\Omega_{\lambda 0} = 0.7$ cosmology and as $(1 + z)^{2.4 \pm 1.0}$ in the Einstein–de Sitter cosmology. The two solid lines overlaid on Figure 6 show the best-fit solutions for each cosmology in the incompleteness-corrected case. The Einstein–de Sitter value is slightly steeper than that obtained by CSB99 (1.3 for $\alpha = -1.0$ and 1.7 for $\alpha = -1.5$) but is consistent within the uncertainties.

Finally, in Figure 7, we compare our values of luminosity density with the values obtained by other surveys. Other groups have previously assumed an Einstein–de Sitter cosmology and therefore should be compared to the triangles from Figure 6. To convert the low-redshift value obtained

TABLE 4
COMOVING 2500 Å ULTRAVIOLET LOGARITHMIC LUMINOSITY DENSITY[a]

			LUMINOSITY DENSITY			
			Flat Lambda		Einstein–de Sitter	
SAMPLE	REDSHIFT	CORRECTED?	$\alpha = -1.0$	$\alpha = -1.5$	$\alpha = -1.0$	$\alpha = -1.5$
U'.....	0.35 ± 0.15	No	26.058	26.211	26.202	26.340
	0.35 ± 0.15	Yes	26.077	26.234	26.223	26.360
B.....	0.80 ± 0.20	No	26.272	26.420	26.491	26.681
	0.80 ± 0.20	Yes	26.339	26.500	26.546	26.746
V.....	1.35 ± 0.25	No	26.284	26.561	26.600	26.871
	1.35 ± 0.25	Yes	26.428	26.712	26.695	26.968

[a] Units are h ergs s^{-1} Hz^{-1} Mpc^{-3}.

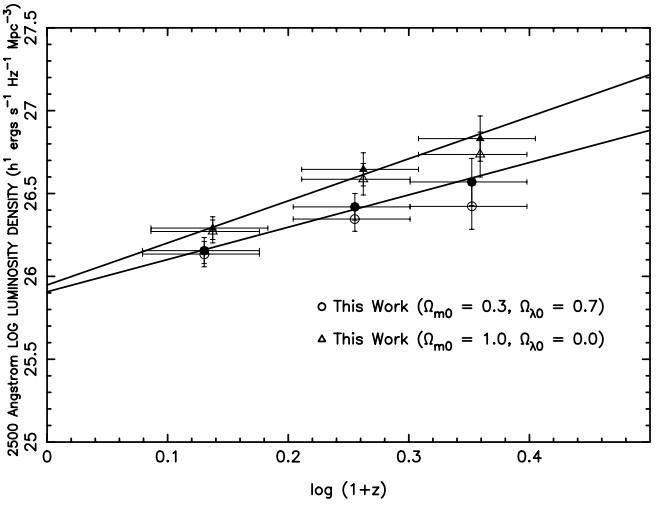

FIG. 6.—Log-log plot of luminosity density vs. $(1 + z)$. The open circles denote the minimal case, and the filled circles denote the incompleteness-corrected case, both for the flat lambda cosmology. The vertical bars show the uncertainties in luminosity density caused by assuming $\alpha = -1.0$ (*bottom*) or $\alpha = -1.5$ (*top*). The triangles show same and are for an Einstein–de Sitter cosmology. They have been offset slightly for clarity. Also shown are the best-fit power law to the incompleteness-corrected values for each cosmology. See § 4 for a discussion of the best power-law fits and Table 5 for the values.

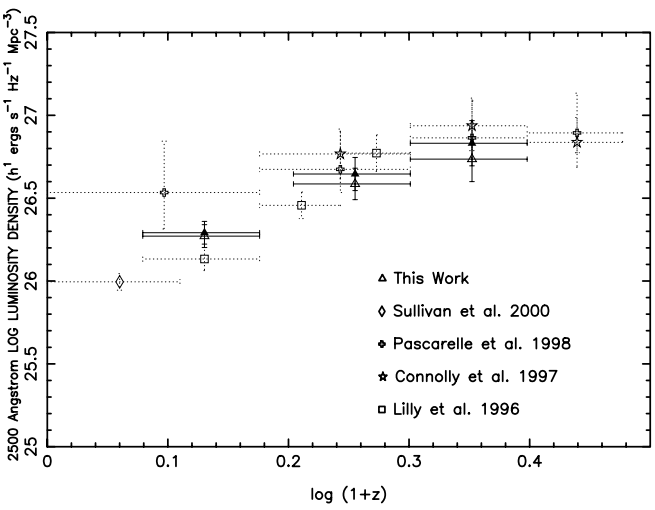

FIG. 7.—Same as Fig. 6, for the Einstein–de Sitter cosmology. The triangles are as in Fig. 6 and denote the minimal (*open*) and incompleteness-corrected (*filled*) case. The vertical bars show the uncertainties in luminosity density caused by assuming $\alpha = -1.0$ or $\alpha = -1.5$. For comparison we have included data points from Lilly et al. (1996, *open squares*), Connolly et al. (1997, *open star*), Pascarelle et al. (1998, *open cross*), and Sullivan et al. (2000, *open diamond*).

by Sullivan et al. (2000; from the FOCA2000 balloon-born survey), we used their best-fit Schechter values (their Table 3) and converted their magnitudes to AB magnitudes using a 2.29 mag offset; we also converted from a rest-frame of 2000 Å to 2500 Å using a $\lambda^{1.1}$ power law, as suggested by Figure 4 of CSB99. As mentioned in § 1, the Sullivan et al. UV-selected sample results in a higher value of integrated luminosity density for the local universe than previous optically derived estimates.

In comparing with the surveys of Pascarelle, Lanzetta, & Fernández-Soto (1998), Connolly et al. (1997), and Lilly et al. (1996), we again converted to a rest frame of 2500 Å using a $\lambda^{1.1}$ power law. We also converted to $H_0 = 100\,h$ km s^{-1} Mpc^{-1}, where necessary. Connolly et al. and Pascarelle et al. both calculate their luminosity density from the small Hubble Deep Field North proper (HDF-N) using photometric redshift estimates. The results of Connolly et al. are more directly comparable to ours, since they measure at a rest frame of 2800 Å, whereas Pascarelle et al. measure at a rest-frame of 1500 Å. Connolly et al. assume a faint-end slope of $\alpha = -1.3$. Both obtain somewhat higher luminosity densities than do we, although the values are consistent within the uncertainties. As discussed at length in the Appendix to CSB99, much of the discrepancy between our results and those of Connolly et al. and Pascarelle et al. may be attributable to the slightly higher number counts in the HDF-N versus other fields.

TABLE 5
BEST-FIT POWER-LAW EXPONENT β

Corrected?	Flat Lambda	Einstein–de Sitter
No	1.44 ± 0.63	2.22 ± 0.62
Yes.....	1.95 ± 0.65	2.54 ± 0.62

Lilly et al. calculated their luminosity density from the Canada-France Redshift Survey, and found a best-fit exponent of $\beta = 3.9 \pm 0.75$. As discussed in § 1, this is somewhat steeper than the value of $\beta = 2.5 \pm 1.0$ that we obtained. From Figure 7, we conclude that the steeper value obtained by Lilly et al. is most likely due to a combination of their $z \sim 1$ luminosity density estimate being higher than ours and their use of a low (optically derived) estimate of the local luminosity density.

In closing, it is important to add one caveat concerning the effect of interstellar dust on our conclusions. In this paper, we assumed that any extinction would suppress UV emission uniformly. This corresponds to applying a constant correction factor to the LFs and does not affect the luminosity density slope inferred from Figure 7. Some authors have suggested that extinction may be luminosity dependent (Adelberger & Steidel 2000; Sullivan et al. 2000; Hopkins et al. 2001). If this is the case, the higher redshift LFs containing greater contributions from brighter galaxies would see larger extinction corrections, possibly flattening the slope observed in Figure 7 from a steeper value. The satisfactory resolution of the complex role of dust and the validity of these claims will require further investigation with larger samples.

5. SUMMARY

We investigated the evolution of the universal rest-frame luminosity density from $z = 1.5$ to the present. The availability of both multicolor data and highly complete spectroscopy enabled us to select galaxies based on their rest-frame ultraviolet color, minimizing potential sources of error such as large K-corrections and interstellar dust. Our large, deep sample allowed us to constrain the faint end of the LF with confidence, even at the highest redshift interval of $z = 1.25 \pm 0.25$. Assuming analytic Schechter forms for

our LFs and using likely extremal faint-end slope values of $\alpha = -1.0$ and $\alpha = -1.5$, we constrained the *relative* luminosity density as a function of redshift. We concluded that, in an $\Omega_{m0} = 0.3$, $\Omega_{\lambda 0} = 0.7$ (Einstein–de Sitter) universe, the evolution in the luminosity density follows a $(1 + z)^{1.7 \pm 1.0}$ $[(1 + z)^{2.4 \pm 1.0}]$ slope from $z = 1.5$ to the present, implying that rather more star formation has occurred in recent times than was previously suggested.

We gratefully acknowledge support from NASA through Hubble Fellowship grant HF-01117.01-A (A. J. B.), awarded by the Space Telescope Science Institute, which is operated by the Association of Universities for Research in Astronomy, Inc., under NASA contract NAS 5-26555; the University of Wisconsin Research Committee with funds granted by the Wisconsin Alumni Research Foundation (A. J. B.); NSF grants AST 00-84847 (A. J. B., principal investigator) and AST 00-84816 (L. L. C.); SAO contract SV4-64008 (D. J. B.); and NASA contract NAS 8-39073 (D. J. B.).

REFERENCES

Adelberger, K. L., & Steidel, C. C. 2000, ApJ, 544, 218
Boyle, B. J., Shanks, T., & Peterson, B. A. 1988, MNRAS, 235, 935
Burstein, D., & Heiles, C. 1984, ApJS, 54, 33
Carlberg, R. G. 1992, ApJ, 399, L31
Cohen, J. G., Hogg, D. W., Blandford, R., Cowie, L. L., Hu, E., Songaila, A., Shopbell, P., & Richberg, K. 2000, ApJ, 538, 29
Connolly, A. J., Szalay, A. S., Dickinson, M., SubbaRao, M. U., & Brunner, R. J. 1997, ApJ, 486, L11
Cowie, L. L., Gardner, J. P., Hu, E. M., Songaila, A., Hodapp, K. W., & Wainscoat, R. J. 1994, ApJ, 434, 114
Cowie, L. L., Songaila, A., & Barger, A. J. 1999, AJ, 118, 603 (CSB99)
Cowie, L. L., Songaila, A., Hu, E. M., & Cohen, J. G. 1996, AJ, 112, 839
Efstathiou, G., Ellis, R. S., & Peterson, B. A. 1988, MNRAS, 232, 431
Ellis, R. S., Colless, M. M., Broadhurst, T. J., Heyl, J. S., & Glazebrook, K. 1996, MNRAS, 280, 235
Felten, J. E. 1976, ApJ, 207, 700
Gardner, J. P., Brown, T. M., & Ferguson, H. C. 2000, ApJ, 542, L79
Gehrels, N. 1986, ApJ, 303, 336
Hogg, D. W., Pahre, M. A., McCarthy, J. K., Cohen, J. G., Blandford, R., Smail, I., & Soifer, B. T. 1997, MNRAS, 288, 404
Hopkins, A. M., Connolly, A. J., Haarsma, D. B., & Cram, L. E. 2001, AJ, 122, 288
Lilly, S. J., Cowie, L. L., & Gardner, J. P. 1991, ApJ, 369, 79
Lilly, S. J., LeFèvre, O., Hammer, F., & Crampton, D. 1996, ApJ, 460, L1
Lilly, S. J., Tresse, L., Hammer, F., Crampton, D., & Le Fevre, O. 1995, ApJ, 455, 108
Luppino, G. 1998, in Optical Detectors in Astronomy, ed. J. W. Beletic & P. Amico (Dordrecht: Kluwer), 83
Madau, P., Ferguson, H. C., Dickinson, M. E., Giavalisco, M., Steidel, C. C., & Fruchter, A. 1996, MNRAS, 283, 1388
Madau, P., Pozzetti, L., & Dickinson, M. 1998, ApJ, 498, 106
Marshall, H. L. 1985, ApJ, 299, 109
Oke, J. B., et al. 1995, PASP, 107, 375
Page, M. J., & Carrera, F. J. 2000, MNRAS, 311, 433
Pascarelle, S. M., Lanzetta, K. M., & Fernández-Soto, A. 1998, ApJ, 508, L1
Pozzetti, L., Madau, P., Zamorani, G., Ferguson, H. C., & Bruzual, G. 1998, MNRAS, 298, 1133
Sandage, A. J., Tammann, G. A., & Yahil, A. 1979, ApJ, 232, 352
Schechter, P. L. 1976, ApJ, 203, 297
Schmidt, M. 1968, ApJ, 151, 393
Sullivan, M., Treyer, M. A., Ellis, R. S., Bridges, T. J., Milliard, B., & Donas, J. 2000, MNRAS, 312, 442
Treyer, M. A., Ellis, R. S., Milliard, B., Donas, J., & Bridges, T. J. 1998, MNRAS, 300, 303
Williams, R. E., et al. 1996, AJ, 112, 1335
Wilson, G., Kaiser, N., Luppino, G. A., & Cowie, L. L. 2001, ApJ, 555, 572